Supplementary Materials for "Measuring topological invariants for higher-order exceptional points in quantum three-mode systems"

Pei-Rong Han[1,2], Wen Ning[1], Xin-Jie Huang[1], Ri-Hua Zheng[1], Shou-Bang Yang[1], Fan Wu[1], Zhen-Biao Yang[1,3],* Qi-Ping Su[4], Chui-Ping Yang[4],† and Shi-Biao Zheng[1,3]‡

[1] *Fujian Key Laboratory of Quantum Information and Quantum Optics, College of Physics and Information Engineering, Fuzhou University, Fuzhou, China*

[2] *School of Physics and Mechanical and Electrical Engineering, Longyan University, Longyan, China*

[3] *Hefei National Laboratory, Hefei, China*

[4] *School of Physics, Hangzhou Normal University, Hangzhou, China*

Contents

S1 . EIGENENERGIES AND EIGENSTATES OF THE NH THREE-MODE SYSTEM

The non-Hermitian (NH) model under consideration involves three modes with nearest-neighbor couplings. The first mode has a non-negligible dissipation rate κ, while dissipation rates of the other two modes are negligible. The system dynamics associated with the no-jump trajectory is governed by the NH Hamiltonian (hereafter setting $\hbar = 1$)

$$H = -\frac{1}{2}i\kappa a_1^\dagger a_1 + \left(\lambda_1 a_1^\dagger a_2 + \lambda_2 a_2^\dagger a_3 + \text{H.c.}\right), \tag{S1}$$

where $a_j^\dagger$ and a_j $(j = 1, ..., 3)$ denote the creation and annihilation operators of the jth mode, λ_j is the coupling coefficient between the jth and $(j+1)$th modes, and H.c. indicates the Hermitian conjugate.

*E-mail: zbyang@fzu.edu.cn
†E-mail: yangcp@hznu.edu.cn
‡E-mail: t96034@fzu.edu.cn

In the single-excitation subspace $\{|1_1 0_2 0_3\rangle, |0_1 1_2 0_3\rangle, |0_1 0_2 1_3\rangle\}$, H has three eigenenergies, given by

$$E_{1,2} = -\frac{i\kappa}{6} - \frac{1}{3}\left[\left(-\frac{1}{2} \mp i\frac{\sqrt{3}}{2}\right)\frac{\xi}{\alpha} + \left(-\frac{1}{2} \pm i\frac{\sqrt{3}}{2}\right)\alpha\right], \tag{S2}$$

and

$$E_3 = -\frac{i\kappa}{6} - \frac{1}{3}\left(\frac{\xi}{\alpha} + \alpha\right), \tag{S3}$$

where

$$\begin{aligned} \xi &= 3\lambda_1^2 + 3\lambda_2^2 - \frac{\kappa^2}{4}, \\ \alpha &= \sqrt[3]{\eta + \sqrt{\eta^2 - \xi^3}}, \end{aligned} \tag{S4}$$

and

$$\eta = -\frac{i\kappa}{4}\left(18\lambda_2^2 - 9\lambda_1^2 + \frac{\kappa^2}{2}\right). \tag{S5}$$

Figure S1(a) illustrates either $\min|\mathrm{Im}(E_n - E_m)|$ or $\min||E_n| - |E_m||$ versus λ_1 and λ_2 scaled in unit of κ. Outside the colored region, $\min|\mathrm{Im}(E_n - E_m)|$ and $\min||E_n| - |E_m||$ are both 0. Considering this in conjunction with Fig. 1b of the main text, it can be concluded that there are at least two eigenenergies with equal imaginary parts and opposite real parts. Therefore, outside this colored region, the eigenenergy can be expressed as

$$\begin{aligned} E_1 &= iI_1, \\ E_2 &= R + iI, \\ E_3 &= -R + iI, \end{aligned} \tag{S6}$$

where R, I, and I_1 are real parameters. Figure S1(b) shows the minimum of the scaled gaps $\min|E_n - E_m|/\kappa$ ($n, m = 1$ to 3, $n \neq m$) among three complex eigenenergies versus λ_1 and λ_2. The curves with $\min|E_n - E_m| = 0$ correspond to lines of EP2s, where two of the three eigenenergies coalesce. The corresponding eigenstates are

$$|\Phi_j\rangle = N_j\left\{\left[E_j\left(E_j + \frac{i\kappa}{2}\right)\right]|0_1 0_2 1_3\rangle + \lambda_2\left(E_j + \frac{i\kappa}{2}\right)|0_1 1_2 0_3\rangle + \lambda_1\lambda_2|1_1 0_2 0_3\rangle\right\} \quad (j = 1, 2, 3), \tag{S7}$$

where N_j is the normalization factor.

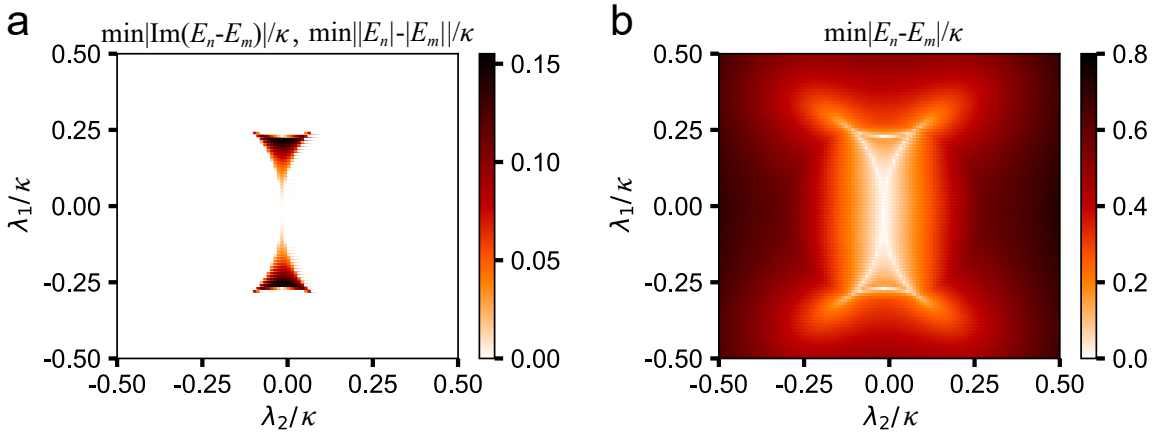

FIG. S1: Characterization of eigenenergies. (a) The colored region is complementary to Fig. 1b in the main text. Outside this region, there is $\min|\mathrm{Im}(E_n - E_m)| = \min||E_n| - |E_m|| = 0$, indicating that at least two eigenenergies have equal imaginary parts and opposite real parts. (b) The lines of 2EPs are highlighted, which corresponds to $\min|E_n - E_m| = 0$.

When $\lambda_1 \neq 0$ and $\lambda_2 \neq 0$, each of these eigenstates is a tripartite entangled state, for which each mode is entangled with the other two modes. The system has four 3EPs at $\{\pm\lambda_1^c, \pm\lambda_2^c\}$ with $\lambda_1^c = \sqrt{2}\kappa/3\sqrt{3}$ and $\lambda_2^c = \kappa/6\sqrt{3}$. For the EP3 in the first quadrant, the three-fold degenerate eigenenergy is

$$E_{\mathrm{EP3}} = -\frac{i\kappa}{6} \tag{S8}$$

with the corresponding eigenstate

$$|\Phi_{\mathrm{EP3}}\rangle = -\sqrt{\frac{1}{6}}|0_1 0_2 1_3\rangle + i\sqrt{\frac{1}{2}}|0_1 1_2 0_3\rangle + \sqrt{\frac{1}{3}}|1_1 0_2 0_3\rangle. \tag{S9}$$

This three-fold degenerate eigenstate is a genuine tripartite entangled state, manifested by the non-zero pairwise concurrences $\mathcal{C}_{1,2} = \sqrt{\frac{2}{3}}$, $\mathcal{C}_{2,3} = \sqrt{\frac{1}{3}}$, and $\mathcal{C}_{1,3} = \sqrt{\frac{2}{9}}$.

S2 . SIMULATION OF CONDITIONAL DYNAMICS IN THE ISOFREQUENCY REGION

After some calculations, we find $\eta^2 - \xi^3 > 0$ in the isofrequency region. Therefore, we can rewrite the parameter α in Eq. S4 as

$$\alpha = (a + ib)^{1/3}, \tag{S10}$$

where $a = \sqrt{\eta^2 - \xi^3}$ and $b = -i\eta$ are real numbers. With this expression, it is easy to check

$$\begin{aligned} |\alpha|^2 &= \left(a^2 + b^2\right)^{1/3} \\ &= -\left(3\lambda_1^2 + 3\lambda_2^2 - \frac{\kappa^2}{4}\right) \\ &= -\xi. \end{aligned} \tag{S11}$$

Then, we obtain $\xi/|\alpha|^2 = -1$. By using $1/\alpha = \alpha^*/|\alpha|^2$, we can further obtain that $\xi/\alpha = -\alpha^*$. Substituting the result into Eq. S2 and Eq. S3, we have

$$E_{1,2} = -\frac{i\kappa}{6} - i\frac{1}{3}\left[\pm\sqrt{3}\mathrm{Re}(\alpha) - \mathrm{Im}(\alpha)\right] \tag{S12}$$

and

$$E_3 = -\frac{i\kappa}{6} - i\frac{2}{3}\mathrm{Im}(\alpha). \tag{S13}$$

Obviously, the result shows that real parts of three eigenenergies vanish in the isofrequency region. Figure S2 shows the simulated evolutions of corresponding eigenstates' fidelities, pairwise concurrences, and the probability for the no-jump trajectory of the initial state $|0_1 0_2 1_3\rangle$ in the region with $\lambda_1/\kappa = 0.2$ and $\lambda_2/\kappa = 0.02$ by using the NH Hamiltonian of Eq. S1. In such a region each of the pairwise concurrences tends to a fixed value for the no-jump case at the price of a progressively decreasing probability.

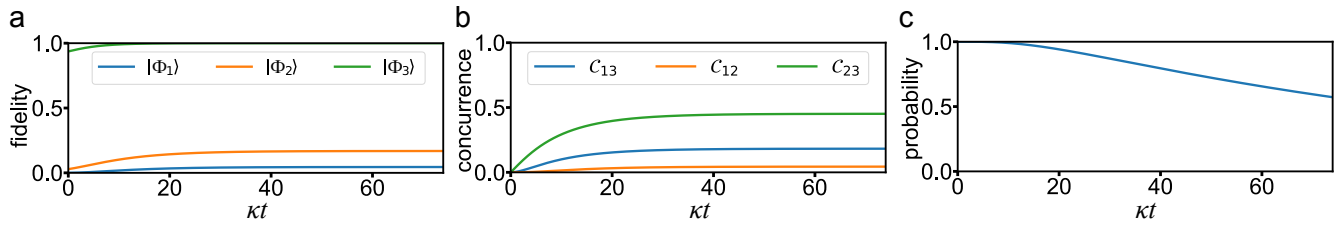

FIG. S2: The fidelity (a), concurrence (b) and probability (c) evolution for the no-jump trajectory of the initial state $|0_1 0_2 1_3\rangle$ with $\lambda_1/\kappa = 0.2$ and $\lambda_2/\kappa = 0.02$. $|\Phi_1\rangle$, $|\Phi_2\rangle$ and $|\Phi_3\rangle$ are the three eigenstates for which the coefficients of the components $|1_1 0_2 0_3\rangle$, $|0_1 1_2 0_3\rangle$ and $|0_1 0_2 1_3\rangle$ have a maximum modulus.

S3 . SYNTHESIS OF THE NH MODEL

The experiment is performed in a circuit quantum electrodynamics architecture involving five frequency-tunable Xmon qubits, each individually coupled to a readout resonator, and all connected to a bus resonator (R_b) with a fixed frequency $\omega_b/2\pi = 5.58$ GHz, as sketched in Fig. S3. Every Xmon qubit used in our experiment has a microwave line (XY line) to drive its state transition and an individual flux line (Z line) to dynamically tune its frequency. The NH three-mode system is synthesized with the bus resonator, one of the Xmon qubits (Q), and its readout resonator (R_r) with a fixed frequency $\omega_r/2\pi = 6.66$ GHz. The R_b-Q and Q-R_r swapping interactions are realized by applying two parametric modulations to Q, making its frequency depend on time as

$$\omega_q = \omega_0 + \varepsilon_1 \cos(\nu_1 t) + \varepsilon_2 \cos(\nu_2 t), \tag{S14}$$

where ω_0 is the mean frequency, and ε_j and ν_j $(j = 1, 2)$ are the corresponding modulation amplitude and angular frequency of the jth modulation, respectively. In the experiment, ε_j and ν_j can be readily manipulated by a Z control line.

Q is capacitively coupled to R_b and R_r (see Ref. [1] for details). The coherent Hamiltonian of the total system is given by

$$H = H_0 + H_I, \tag{S15}$$

where

$$H_0 = \omega_b a_b^\dagger a_b + \omega_r a_r^\dagger a_r + \omega_q |e\rangle\langle e|, \tag{S16}$$

and

$$H_I = |0_q\rangle\langle 1_q| \left(g_b a_b^\dagger + g_r a_r^\dagger\right) + \text{H.c.}, \tag{S17}$$

where $a_r^\dagger$ $(a_b^\dagger)$ and a_r (a_b) denote the creation and annihilation operators for the photonic field stored in R_r (R_b), $|0_q\rangle$ and $|1_q\rangle$ denote the ground and first excited states of Q, and g_b (g_r) is the on-resonance R_b-Q (Q-R_r) coupling strength.

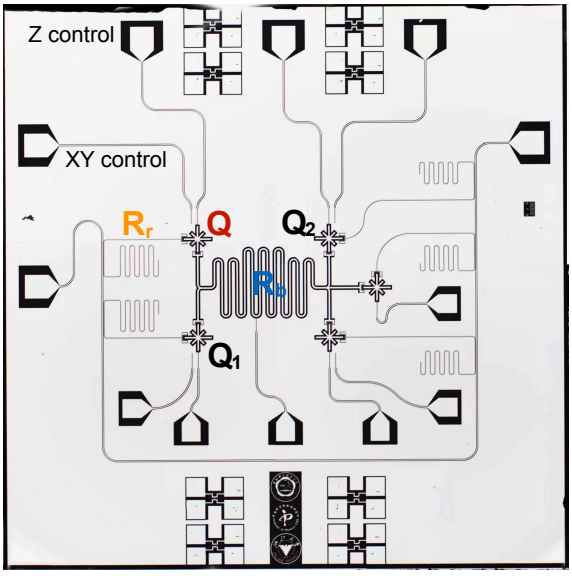

FIG. S3: Circuit micrography.

Performing the transformation $e^{i\int_0^t H_0 dt}$, we obtain the system Hamiltonian in the interaction picture,

$$H_I' = e^{-i\mu_1 \sin(\nu_1 t)} e^{-i\mu_2 \sin(\nu_2 t)} |0_q\rangle\langle 1_q| \left(e^{i\delta_b t} g_b a_b^\dagger + e^{i\delta_r t} g_r a_r^\dagger\right) + \text{H.c.}, \tag{S18}$$

where $\mu_j = \varepsilon_j/\nu_j$ $(j = 1, 2)$, $\delta_b = \omega_b - \omega_0$, and $\delta_r = \omega_r - \omega_0$. Using the Jacobi-Anger expansion

$$e^{-i\mu_j \sin(\nu_j t)} = \sum_{n=-\infty}^{\infty} J_n(\mu_j) e^{-in\nu_j t}, \tag{S19}$$

with $J_n(\mu_j)$ being the nth Bessel function of the first kind, H_I' can be rewritten as

$$H_I' = \sum_{m,n=-\infty}^{\infty} J_m(\mu_1) J_n(\mu_2) e^{-im\nu_1 t} e^{-in\nu_2 t} |0_q\rangle \langle 1_q| \left(e^{i\delta_b t} g_b a_b^\dagger + e^{i\delta_r t} g_r a_r^\dagger \right) + \text{H.c.} \tag{S20}$$

Under the conditions $\nu_1 = \delta_r$ and $\nu_2 = -\delta_b$, Q is resonantly coupled to R_r (R_b) at the first upper (lower) sideband with respect to the first (second) modulation. When $g_b, g_r \ll \nu_1, \nu_2$, the fast-oscillating terms can be discarded, so that H_I' reduces to

$$H_I' = |0_q\rangle \langle 1_q| \left(\lambda_1 a_b^\dagger + \lambda_2 a_r^\dagger \right) + \text{H.c.}, \tag{S21}$$

where $\lambda_1 = g_r J_1(\mu_1) J_0(\mu_2)$ and $\lambda_2 = g_b J_0(\mu_1) J_1(\mu_2)$, as depicted in Fig. 2a of the main text. In the single-excitation subspace, $a_b^\dagger$ and $a_r^\dagger$ can be replaced by $|1_b\rangle \langle 0_b|$ and $|1_r\rangle \langle 0_r|$, respectively. Then H_I' is equivalent to the Hermitian part of the Hamiltonian (1) of the main text with $N = 3$. In our system, the dissipation rates of R_b and Q are respectively 0.08 MHz and 0.06 MHz, which are negligible compared with that of R_r. With the dissipation being included, the NH Hamiltonian is given by Eq. S1, with R_r, Q, and R_b corresponding to the first, second, and last qubits, respectively.

S4 . STATE READOUT

The readout of the output R_b-Q-R_r state is enabled with two ancilla qubits, denoted as Q_1 and Q_2. After the NH Hamiltonian dynamics, the state of R_b is mapped to Q_1 through a swapping gate, which is realized by tuning the transition frequency of Q_1 to ω_b for a duration $t_{sw} = \pi/(2g_1) \simeq 12.3\ ns$, with $g_1 = 2\pi \times 20.3$ MHz being the R_b-Q photonic swapping rate. Then, the state of Q is transferred to Q_2 by subsequently performing the Q-R_b and R_b-Q_2 swapping gates. Finally, R_r's state is transferred to Q. As the maximum frequency of Q ($2\pi \times 6.01$ GHz) is smaller than ω_r by an amount much lager than g_r, it is necessary to use the parametric modulation to realize the R_r-Q mapping. The corresponding gate duration is 150 ns. With a correction for the state distortion during the state mapping, the resulting Q_1-Q_2-Q output state corresponds to the R_b-Q-R_r output state right before the state mapping.

S5 . EXTRACTION OF EIGENENERGIES

In our experiment, we choose a square-shaped loop on the λ_1-λ_2 plane to extract the winding number. The four vertices of the rectangle are $(0,0)$, $(\lambda_m, 0)$, $(0, \lambda_m)$, and (λ_m, λ_m) with $\lambda_m \simeq 2\pi \times 1$ MHz. Along the edge with $\lambda_1 = 0$, R_r is decoupled from the Q-R_b subsystem. In the interaction picture, the Q-R_b swapping coupling is described by the Hamiltonian

$$\mathcal{H} = \lambda_2 \left(a_b^\dagger |0_q\rangle \langle 1_q| + a_b |1_q\rangle \langle 0_q| \right), \tag{S22}$$

where $a_b^\dagger$ and a_b denote the creation and annihilation operators for the photonic mode stored in R_b, and $|0_q\rangle$ and $|1_q\rangle$ represent the ground and excited states of Q. In the single-excitation subspace, this Hamiltonian has two eigenenergies $E_\pm = \pm\lambda_2$. The corresponding eigenstates are

$$|\Phi_\pm\rangle = \frac{1}{\sqrt{2}} \left(|0_b 1_q\rangle \pm |1_b 0_q\rangle \right). \tag{S23}$$

The subsystem, starting from the initial state $|0_b 1_q\rangle$, evolves as

$$\cos(\lambda_2 t) |0_b 1_q\rangle - i \sin(\lambda_2 t) |1_b 0_q\rangle. \tag{S24}$$

The value of λ_2, which depends on the amplitude and frequency of the parametric modulation used to mediate the sideband interaction, is inferred from the observed Rabi oscillation. The population evolutions for the state $|0_b 1_q\rangle$,

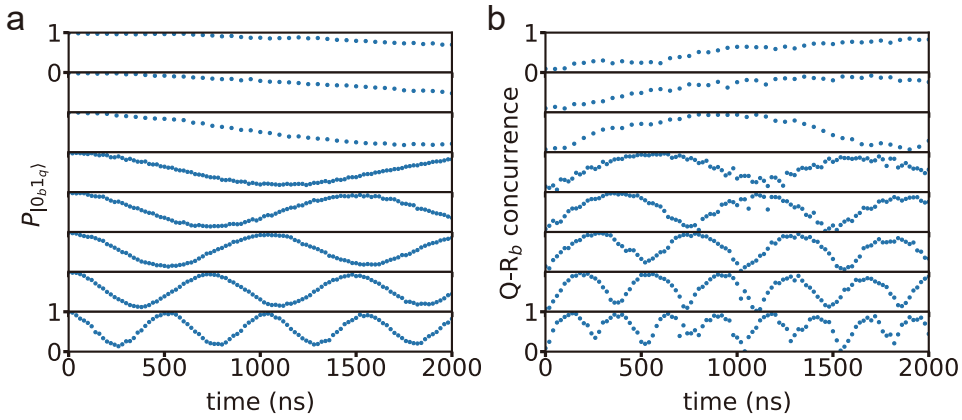

FIG. S4: The population (a) and concurrence (b) evolutions for different values of λ_2 when $\lambda_1 = 0$, i.e., the edge from $(0,0)$ to $(0,\lambda_m)$. From top to bottom, the values of $\lambda_2/2\pi$ are 0.04, 0.05, 0.14, 0.23, 0.33, 0.48, 0.68 and 0.97 MHz, respectively.

observed for different values of λ_2, are presented in Fig. S4(a). The Q-R_b concurrences associated with the two eigenstates $|\Phi_\pm\rangle$, extracted at $\lambda_2 = \lambda_m$, are 0.997 and 0.997, respectively.

For $\lambda_2 = 0$, R_b is decoupled from the Q-R_r subsystem. In this case, the evolution of the Q-R_r subsystem associated with the no-jump trajectory is described by the NH Hamiltonian

$$\mathcal{H}' = \lambda_1 \left(a_r^\dagger |0_q\rangle \langle 1_q| + a_r |1_q\rangle \langle 0_q| \right) - \frac{i}{2}\kappa a_r^\dagger a_r, \tag{S25}$$

where $a_r^\dagger$ (a_r) is the photonic creation (annihilation) operator for R_r. In the single-excitation subspace, the $\mathcal{H}'$ has two eigenenergies

$$E'_\pm = -i\kappa/4 \pm \sqrt{\lambda_1^2 - \kappa^2/16}. \tag{S26}$$

The corresponding eigenstates are

$$|\Phi'_\pm\rangle = \mathcal{N}_\pm \left(|1_q 0_r\rangle + \frac{E'_\pm}{\lambda_1} |0_q 1_r\rangle \right), \tag{S27}$$

where $\mathcal{N}_\pm = \left(1 + \left|E'_\pm/\lambda_1\right|^2\right)^{-1/2}$. Fig. S5(a) shows the measured population of the state $|1_q 0_r\rangle$ versus λ_1 and t. This population is obtained by discarding the outcome $|0_q 0_r\rangle$, and then renormalizing the probabilities for the outcomes of $|1_q 0_r\rangle$ and $|0_q 1_r\rangle$. The gap of the two eigenenergies versus λ_1, extracted from the population evolution, are shown in Fig. S5(c).

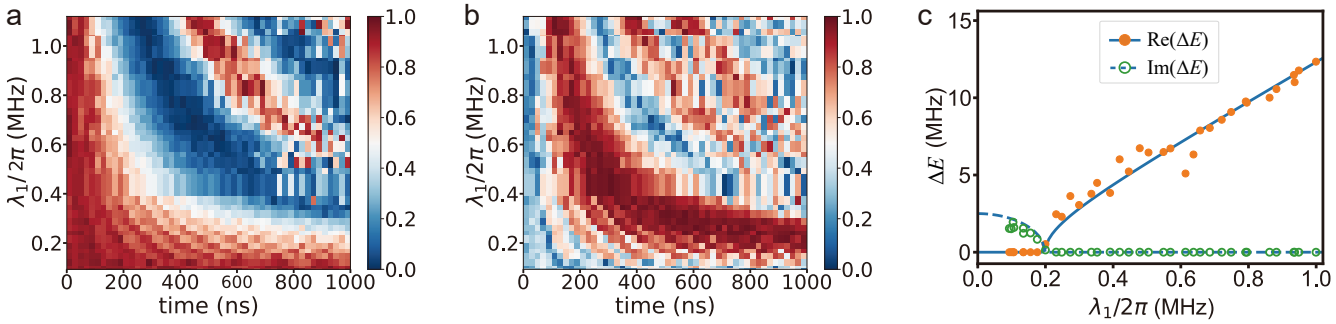

FIG. S5: The population (a) and concurrence (b) evolutions for different values of λ_1 when $\lambda_2 = 0$, i.e., the edge from $(0,0)$ to $(\lambda_m,0)$. (c) Spectral gap ΔE. The solid and dashed lines denote the real and imaginary parts, respectively.

When $\lambda_1 \neq 0$ and $\lambda_2 \neq 0$, the evolution of the R_b-Q-R_r system associated with the no-jump trajectory is governed by the Hamiltonian

$$\mathcal{H} = \mathcal{H}^H + \mathcal{H}^{NH}, \tag{S28}$$

where

$$\begin{aligned} \mathcal{H}^H &= |1_q\rangle \langle 0_q| (\lambda_1 a_r + \lambda_2 a_b) + \text{H.c.}, \\ \mathcal{H}^{NH} &= -\frac{1}{2} i\kappa a_r^\dagger a_r. \end{aligned} \tag{S29}$$

Suppose that the loop on the $\lambda_1 - \lambda_2$ plane is a rectangle with four vertices $(0,0)$, $(\lambda_m, 0)$, $(0, \lambda_m)$, and (λ_m, λ_m). On the edges from $(0,0)$ to $(\lambda_m, 0)$ and to $(0, \lambda_m)$, the system reduces to a two-mode system, so that the eigenspectra can be extracted relatively easily. Without dissipation, the three eigenstates of $\mathcal{H}^H$ on the other two edges are given by

$$\begin{aligned} |\Phi_1\rangle &= \sin\theta\, |1_b 0_q 0_r\rangle - \cos\theta\, |0_b 0_q 1_r\rangle\,, \\ |\Phi_2\rangle &= \frac{1}{\sqrt{2}}(\cos\theta\, |1_b 0_q 0_r\rangle + \sin\theta\, |0_b 0_q 1_r\rangle + |0_b 1_q 0_r\rangle), \\ |\Phi_3\rangle &= \frac{1}{\sqrt{2}}(\cos\theta\, |1_b 0_q 0_r\rangle + \sin\theta\, |0_b 0_q 1_r\rangle - |0_b 1_q 0_r\rangle), \end{aligned} \tag{S30}$$

where $\tan\theta = \lambda_1/\lambda_2$. The corresponding eigenenergies are $E_1^H = 0$ and $E_2^H = -E_3^H = \lambda$, with $\lambda = \sqrt{\lambda_1^2 + \lambda_2^2}$.

In the basis $\{|\Phi_j\rangle\}$ $(j = 1, 2, 3)$, $\mathcal{H}^{NH}$ can be expressed as

$$\mathcal{H}^{NH} = \mathcal{H}^{dg} + \mathcal{H}^{ndg}, \tag{S31}$$

where $\mathcal{H}^{dg}$ and $\mathcal{H}^{ndg}$ represent the diagonal and off-diagonal parts respectively, given by

$$\mathcal{H}^{dg} = \begin{pmatrix} -i\frac{\kappa}{2}\cos^2\theta & 0 & 0 \\ 0 & -i\frac{\kappa}{4}\sin^2\theta & 0 \\ 0 & 0 & -i\frac{\kappa}{4}\sin^2\theta \end{pmatrix}, \tag{S32}$$

and

$$\mathcal{H}^{ndg} = \begin{pmatrix} 0 & i\frac{\kappa}{4\sqrt{2}}\sin(2\theta) & i\frac{\kappa}{4\sqrt{2}}\sin(2\theta) \\ i\frac{\kappa}{4\sqrt{2}}\sin(2\theta) & 0 & i\frac{\kappa}{4}\sin^2\theta \\ i\frac{\kappa}{4\sqrt{2}}\sin(2\theta) & i\frac{\kappa}{4}\sin^2\theta & 0 \end{pmatrix}. \tag{S33}$$

In the basis $\{|\Phi_j\rangle\}$, we can rewrite the total Hamiltonian as

$$\mathcal{H} = \mathcal{H}^0 + \mathcal{H}^{ndg}, \tag{S34}$$

where

$$\begin{aligned} \mathcal{H}^0 &= \mathcal{H}^H + \mathcal{H}^{dg} \\ &= \begin{pmatrix} -i\frac{\kappa}{2}\cos^2\theta & 0 & 0 \\ 0 & \lambda - i\frac{\kappa}{4}\sin^2\theta & 0 \\ 0 & 0 & -\lambda - i\frac{\kappa}{4}\sin^2\theta \end{pmatrix}. \end{aligned} \tag{S35}$$

We note $\mathcal{H}^{ndg}$ can be treated as a perturbation, which is explained as follow. On the edge with $\lambda_1 = \lambda_m$, θ changes from $\pi/2$ to $\pi/4$. For $\theta = \pi/2$, the non-zero off-diagonal elements are $\mathcal{H}_{2,3}^{ndg}$ and $H_{3,2}^{ndg}$, which have a magnitude of $\left|\mathcal{H}_{2,3}^{ndg}\right| = \kappa/4$. The ratio of this magnitude to the gap between the last two eigenvalues of $\mathcal{H}^0$ is $\left|\mathcal{H}_{2,3}^{ndg}\right| / \left|\mathcal{H}_{2,2}^0 - \mathcal{H}_{3,3}^0\right| = \kappa/8\lambda \simeq 0.099$. When θ changes to $\pi/4$, $\left|\mathcal{H}_{2,3}^{ndg}\right| / \left|\mathcal{H}_{2,2}^0 - \mathcal{H}_{3,3}^0\right|$ monotonously decreases to 0.070, while $\left|\mathcal{H}_{1,2}^{ndg}\right| / \left|\mathcal{H}_{1,1}^0 - \mathcal{H}_{2,2}^0\right|$ approximately increases to $\kappa/(4\sqrt{2}\lambda) \simeq 0.099$. On the edge with $\lambda_2 = \lambda_m$, θ changes from 0 to $\pi/4$. For $\theta = 0$, all the off-diagonal elements are 0. When θ increases to $\pi/4$, $\left|\mathcal{H}_{1,2}^{ndg}\right| / \left|\mathcal{H}_{1,1}^0 - \mathcal{H}_{2,2}^0\right|$

and $\left|\mathcal{H}^{ndg}_{2,3}\right| / \left|\mathcal{H}^{0}_{2,2} - \mathcal{H}^{0}_{3,3}\right|$ approximately increase to 0.098 and 0.099, respectively. These results imply that the magnitude of each off-diagonal element is much smaller than the corresponding energy gap, which ensures the perturbation condition. To the first order correction, the three eigenenergies correspond to the diagonal elements of $\mathcal{H}^0$. This indicates that the real part of the first eigenenergy E_1 is approximately zero, and the other two eigenenergies E_2 and E_3 have the same imaginary part but opposite real parts. Therefore, the three eigenenergies can be approximately expressed as

$$\begin{aligned} E_1 &\simeq -iI_1, \\ E_2 &\simeq R - iI_2, \\ E_3 &\simeq -R - iI_2, \end{aligned} \tag{S36}$$

where R, I_1, and I_2 are real parameters, with $I_1 = \frac{\kappa}{2}\cos^2\theta$ and $I_2 = \frac{\kappa}{4}\sin^2\theta$. Consequently, the eigenenergies are determined by these three parameters $\{R,\ I_1,\ I_2\}$, which can be extracted through observation of the population evolutions.

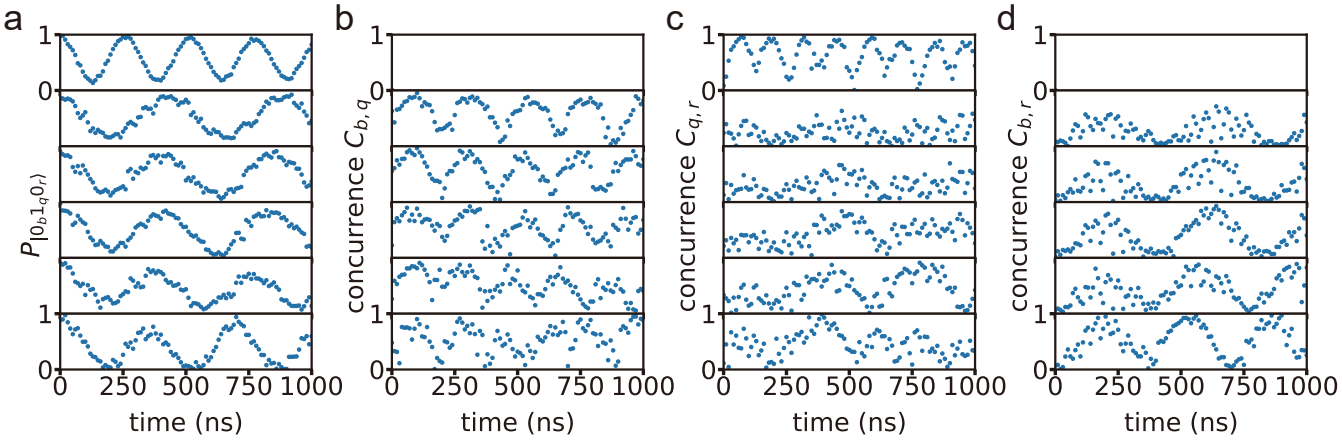

FIG. S6: The population (a) and concurrence (b),(c),(d) evolutions for different values of λ_1 when $\lambda_2 = \lambda_m$, i.e., the edge from $(0, \lambda_m)$ to (λ_m, λ_m). From top to bottom, the values of $\lambda_1/2\pi$ are 0, 0.49, 0.58, 0.77, 0.83 and 1.01 MHz, respectively.

Figure S6(a) displays the measured population of the state $|0_b1_q0_r\rangle$ versus λ_1 and t for the edge with $\lambda_2 = \lambda_m$. This population is obtained by discarding the outcome $|0_b0_q0_r\rangle$, and then renormalizing the probabilities of the three single-excitation outcomes. The eigenenergies in terms of R and ΔI $(= |I_1 - I_2|)$ versus λ_1, extracted from this population evolution, are displayed in Fig. S7(a). Figure S10(a) shows the measured $|0_b1_q0_r\rangle$-state population versus λ_2 and t for the edge with $\lambda_1 = \lambda_m$. The extracted eigenenergies in terms of R and ΔI versus λ_2 are displayed in Fig. S7(b).

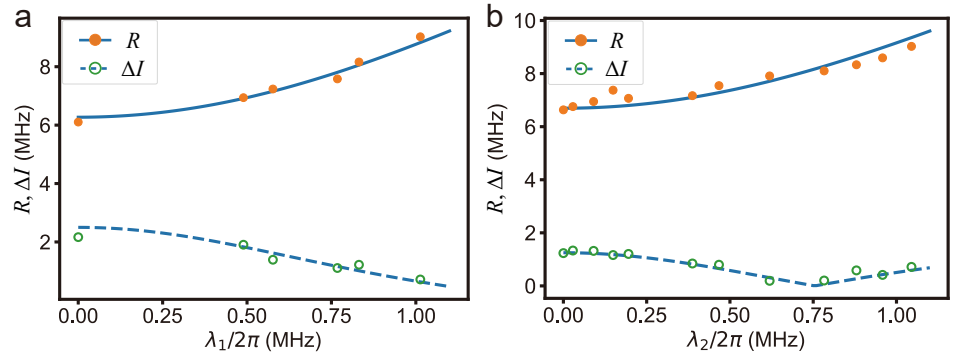

FIG. S7: The extracted eigenenergies in terms of R and ΔI versus (a) λ_1 and (b) λ_2.

S6 . CHARACTERIZATION OF THE NONCLASSICALITY

Along the edge with $\lambda_1 = 0$, R_r remains in the ground state $|0_r\rangle$. The measured Q-R_b concurrence, versus λ_2 and t, is displayed in Fig. S4(b). The density matrices for the two eigenstates $|\Phi_\pm\rangle$, extracted from the data measured at $\lambda_2 = \lambda_m$, are presented in Fig. S8. The concurrences corresponding to these two eigenstates are 0.997 and 0.997, respectively. Fig. S5(b) shows the Q-R_r concurrence versus λ_1 and t, measured for the edge $\lambda_2 = 0$. The measured density matrices, associated with the two eigenstates $|\Phi'_\pm\rangle$ for $\lambda_1 = \lambda_m$, are presented in Fig. S9, with the concurrences 0.971 and 0.971.

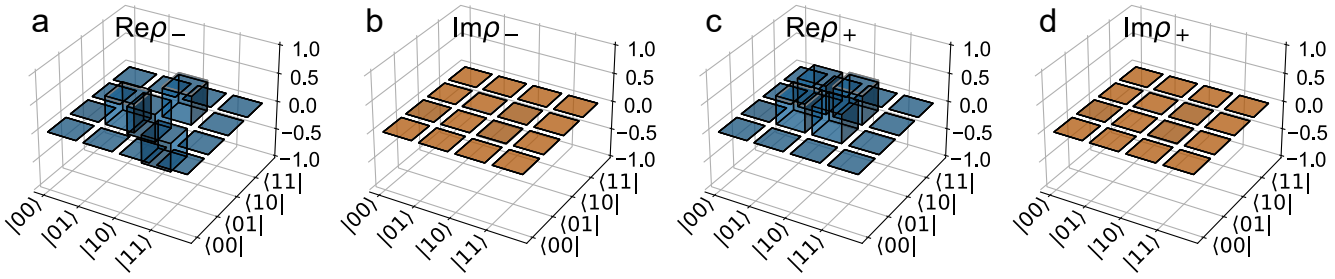

FIG. S8: The density matrices $\rho_\pm$ for the two eigenstates $|\Phi_\pm\rangle$. (a) The real parts of ρ_-. (b) The imaginary parts of ρ_-. (c) The real parts of ρ_+. (d) The imaginary parts of ρ_+. The two numbers in each ket denote the excitation numbers of the qubit and the bus resonator, respectively. The black frames denote the matrix elements of the ideal eigenstates.

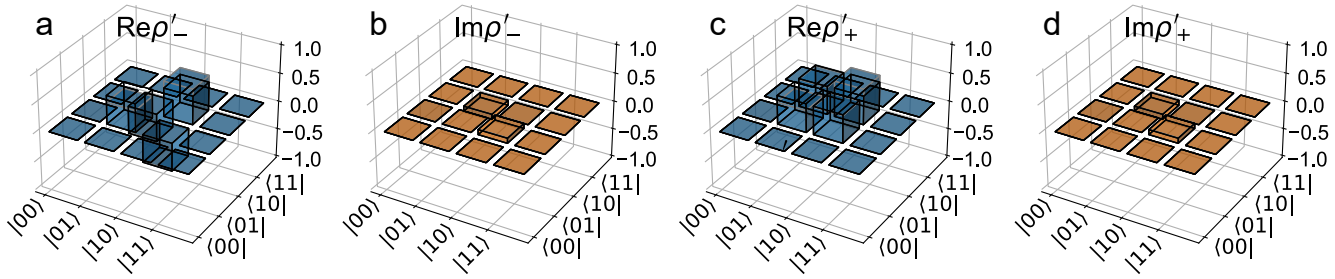

FIG. S9: The density matrices $\rho'_\pm$ for the two eigenstates $|\Phi'_\pm\rangle$. (a) The real parts of ρ'_-. (b) The imaginary parts of ρ'_-. (c) The real parts of ρ'_+. (d) The imaginary parts of ρ'_+. The two numbers in each ket denote the excitation numbers of the qubit and the readout resonator, respectively. The black frames denote the matrix elements of the ideal eigenstates.

Figures S6(b), (c), and (d) present the measured three pairwise concurrences $C_{b,q}$, $C_{q,r}$, and $C_{b,r}$ versus λ_1 and t for the edge with $\lambda_2 = \lambda_m$, where the subscript "b", "q", and "r" denote the bus resonator, Xmon qubit, and readout resonator, respectively. Figure S10(b), (c), and (d) showcase the three pairwise concurrences versus λ_2 and t for the edge with $\lambda_1 = \lambda_m$. These results show that the tripartite system evolves from the initial product state $|0_b 1_q 0_r\rangle$ to a tripartite entangled state under the NH Hamiltonian when $\lambda_1 \neq 0$ and $\lambda_2 \neq 0$. For example, the three concurrences, measured at the point with $\lambda_1 = \lambda_2 = \lambda_m$ for the time 600 ns, are $C_{b,q} = 0.50$, $C_{q,r} = 0.64$, and $C_{b,r} = 0.74$, respectively. These results imply that the corresponding eigenstates are highly-nonclassical states, featuring tripartite quantum entanglement.

S7 . DERIVATION OF THE RESULTANT VECTOR

The resultant is a basic concept in algebra. It can be used to determine whether two polynomials have common roots, defined as

$$R_{P_1,P_2} \equiv \det S_{P_1,P_2}, \tag{S37}$$

where P_1, P_2 are two polynomials and S_{P_1,P_2} is their Sylvester matrix. Suppose

$$\begin{aligned} P_1 &= a_0 x^n + a_1 x^{n-1} + ... + a_n, \\ P_2 &= b_0 x^m + b_1 x^{m-1} + ... + b_m, \end{aligned} \tag{S38}$$

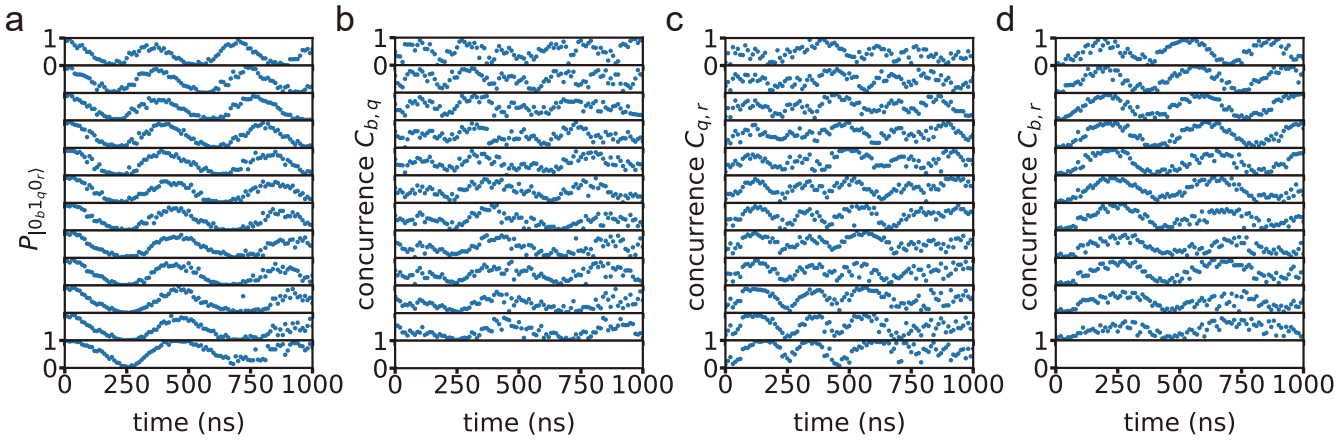

FIG. S10: The population (a) and concurrence (b),(c),(d) evolutions for different values of λ_2 when $\lambda_1 = \lambda_m$, i.e., the edge from $(\lambda_m, 0)$ to (λ_m, λ_m). From top to bottom, the values of $\lambda_2/2\pi$ are 1.04, 0.96, 0.88, 0.78, 0.62, 0.47, 0.39, 0.20, 0.15, 0.09, 0.03 and 0 MHz, respectively.

the corresponding resultant is a determinant of order $m+n$,

$$R_{P_1,P_2} = \begin{vmatrix} a_0 & a_1 & a_2 & \dots & \dots & a_n & 0 & \dots & 0 \\ 0 & a_0 & a_1 & \dots & \dots & a_{n-1} & a_n & \dots & 0 \\ \vdots & \vdots & \vdots & \vdots & \vdots & \vdots & \vdots & \vdots & \vdots \\ 0 & 0 & \dots & 0 & a_0 & \dots & \dots & \dots & a_n \\ b_0 & b_1 & b_2 & \dots & \dots & \dots & b_m & \dots & 0 \\ 0 & b_0 & b_1 & \dots & \dots & \dots & b_{m-1} & b_m & \dots \\ \vdots & \vdots & \vdots & \vdots & \vdots & \vdots & \vdots & \vdots & \vdots \\ 0 & \dots & 0 & b_0 & b_1 & \dots & \dots & \dots & b_m \end{vmatrix}. \tag{S39}$$

If $R_{P_1,P_2} = 0$, the polynomials P_1 and P_2 have common roots.

For a three-dimensional system governed by the Hamiltonian H, the characteristic polynomial P is given by

$$P = -(E - E_1)(E - E_2)(E - E_3), \tag{S40}$$

where E_1, E_2 and E_3 are the three eigenvalues of H. The first- and second-order derivatives of $P(E)$ are

$$P' = -[(E - E_1)(E - E_2) + (E - E_2)(E - E_3) + (E - E_3)(E - E_1)], \tag{S41}$$

and

$$P'' = -2[(E - E_1) + (E - E_2) + (E - E_3)]. \tag{S42}$$

The two components of the resultant vector are given by

$$\mathcal{R}_1 = -R_{P,P'} = (E_1 - E_2)^2(E_1 - E_3)^2(E_2 - E_3)^2 \tag{S43}$$

and

$$\mathcal{R}_2 = iR_{P,P''} = 8(E_1 + E_3 - 2E_2)(E_1 + E_2 - 2E_3)(E_2 + E_3 - 2E_1). \tag{S44}$$

Therefore, we can calculate $\mathcal{R}_1$ and $\mathcal{R}_2$ at each point (λ_1, λ_2) of the parameter space with the measured eigenenergies. The results are presented in Fig. 3 of the main text.

S8 . EXTRACTION OF THE WINDING NUMBER

The winding number, associated with each EP3, is calculated along a loop enclosing the EP3,

$$\mathcal{W} = \frac{1}{2\pi} \sum_{j=1,2} \oint_{C_\lambda} F(\mathcal{R}_1, \mathcal{R}_2) d\lambda_j, \tag{S45}$$

where the integrand is given by

$$F(\mathcal{R}_1,\mathcal{R}_2)=\frac{1}{\|\mathcal{R}\|^2}\left(\mathcal{R}_1\frac{\partial\mathcal{R}_2}{\partial\lambda_j}-\mathcal{R}_2\frac{\partial\mathcal{R}_1}{\partial\lambda_j}\right). \tag{S46}$$

The square-shaped loop chosen in our experiment encloses the EP3 in the first quadrant. Only one control parameter changes along each edge of the loop. Thus the integral can be rewritten as

$$\begin{aligned}\mathcal{W}=&\frac{1}{2\pi}\int_0^{\lambda_m}F(\mathcal{R}_1,\mathcal{R}_2)d\lambda_1|_{\lambda_2=0}\\&+\frac{1}{2\pi}\int_0^{\lambda_m}F(\mathcal{R}_1,\mathcal{R}_2)d\lambda_2|_{\lambda_1=\lambda_m}\\&+\frac{1}{2\pi}\int_{\lambda_m}^{0}F(\mathcal{R}_1,\mathcal{R}_2)d\lambda_1|_{\lambda_2=\lambda_m}\\&+\frac{1}{2\pi}\int_{\lambda_m}^{0}F(\mathcal{R}_1,\mathcal{R}_2)d\lambda_2|_{\lambda_1=0},\end{aligned} \tag{S47}$$

where $F(\mathcal{R}_1,\mathcal{R}_2)$ along the four edges are displayed in Fig. S11.

For simplicity, the square-shaped trajectory can be represented by the parametric equation

$$\begin{aligned}\lambda_1&=\frac{1}{2}\left(1-\cos\theta|\cos\theta|+\sin\theta|\sin\theta|\right),\\\lambda_2&=\frac{1}{2}\left(1-\cos\theta|\cos\theta|-\sin\theta|\sin\theta|\right),\end{aligned} \tag{S48}$$

where θ ranges from 0 to 2π. In this case, the winding number in terms of θ is given by

$$\mathcal{W}=\frac{1}{2\pi}\int_0^{2\pi}\frac{1}{\|\mathcal{R}\|^2}\left(\mathcal{R}_1\frac{\partial\mathcal{R}_2}{\partial\theta}-\mathcal{R}_2\frac{\partial\mathcal{R}_1}{\partial\theta}\right)d\theta. \tag{S49}$$

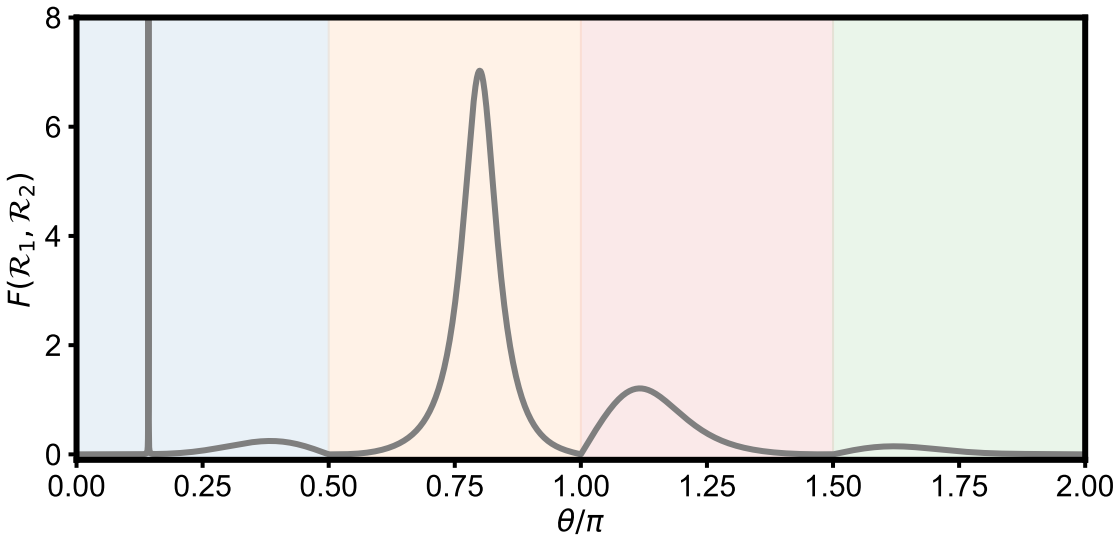

FIG. S11: $F(\mathcal{R}_1,\mathcal{R}_2)$ along the four edges. Areas with different background colors correspond to the four edges.

S9 . WINDING NUMBERS FOR DPS AND EP2S

To confirm that the winding number, defined by Eq.3 of the main text, is indeed uniquely associated with the topology for the three-order EPs, we here calculate this quantity for the DPs (diabolical points) in both the two-dimensional (2D) and 3D Hermitian system, as well as for the EP2s in a 2D NH system.

We first consider the 2D Hermitian system with the Hamiltonian $H = \omega_x\sigma_x + \omega_y\sigma_y$, where ω_x (ω_y) is a real number. This model admits two real eigenenergies, and one could study the DP at $\omega_x = \omega_y = 0$. The characteristic polynomial of H is

$$P(E) = E^2 - (\omega_x^2 + \omega_y^2), \tag{S50}$$

and its first-order derivative is

$$P'(E) = 2E. \tag{S51}$$

The second-order derivative of $P(E)$ is a constant, $P''(E) = 2$. In order to construct the Sylvester matrix of $P(E)$ and $P''(E)$, we can take $P''(E)$ as a polynomial of degree 1 with a zero coefficient,

$$P''(E) = 2 + 0E. \tag{S52}$$

In this way, we have

$$S_{P,P'} = \begin{pmatrix} 1 & 0 & -(\omega_x^2+\omega_y^2) \\ 2 & 0 & 0 \\ 0 & 2 & 0 \end{pmatrix} \text{ and } S_{P,P''} = \begin{pmatrix} 1 & 0 & -(\omega_x^2+\omega_y^2) \\ 0 & 2 & 0 \\ 0 & 0 & 2 \end{pmatrix}. \tag{S53}$$

The corresponding resultant $\mathcal{R}_1 = R_{P,P'} \equiv \det S_{P,P'} = 1 - 4(\omega_x^2 + \omega_y^2)$ is a real-valued function, while $\mathcal{R}_2 = R_{P,P''} \equiv \det S_{P,P''} = 4$ is a constant. Therefore, along a closed loop around DP in a 2D space spanned by ω_x and ω_y, the trajectory of resultant vector $\mathcal{R}$ in the $\mathcal{R}_1 - \mathcal{R}_2$ plane is a line segment instead of a closed curve, which means the winding number is always 0. We further note that the spectrum of any 2D Hermitian system has a similar structure, so that the corresponding winding number is zero.

We now turn to the 3D Hermitian system, whose dynamics is described by the three-mode Hamiltonian of Eq. S1 with $\kappa = 0$. In the single-excitation subspace, the Hamiltonian takes the form

$$H = \begin{pmatrix} 0 & \lambda_2 & 0 \\ \lambda_2 & 0 & \lambda_1 \\ 0 & \lambda_1 & 0 \end{pmatrix}, \tag{S54}$$

with a DP at $\lambda_1 = \lambda_2 = 0$. The characteristic polynomial reads

$$P(E) = -E^3 + (\lambda_1^2 + \lambda_2^2)E \tag{S55}$$

and its derivatives are

$$P'(E) = -3E^2 + (\lambda_1^2 + \lambda_2^2), \tag{S56}$$

$$P''(E) = -6E. \tag{S57}$$

We then have

$$S_{P,P'} = \begin{pmatrix} -1 & 0 & \lambda_1^2+\lambda_2^2 & 0 & 0 \\ 0 & -1 & 0 & \lambda_1^2+\lambda_2^2 & 0 \\ -3 & 0 & \lambda_1^2+\lambda_2^2 & 0 & 0 \\ 0 & -3 & 0 & \lambda_1^2+\lambda_2^2 & 0 \\ 0 & 0 & -3 & 0 & \lambda_1^2+\lambda_2^2 \end{pmatrix} \tag{S58}$$

and

$$S_{P,P''} = \begin{pmatrix} -1 & 0 & \lambda_1^2+\lambda_2^2 & 0 \\ -6 & 0 & 0 & 0 \\ 0 & -6 & 0 & 0 \\ 0 & 0 & -6 & 0 \end{pmatrix}. \tag{S59}$$

The corresponding resultants are

$$\begin{aligned} \mathcal{R}_1 = R_{P,P'} &\equiv \det S_{P,P'} \\ &= 4\lambda_2^6 + 12\lambda_2^4\lambda_1^2 + 12\lambda_2^2\lambda_1^4 + 4\lambda_1^6 \end{aligned} \tag{S60}$$

and

$$\begin{aligned}\mathcal{R}_2 &= R_{P,P''} \equiv \det S_{P,P''} \\ &= 0.\end{aligned} \tag{S61}$$

Similar to *Example 1*, $\mathcal{R}_1$ is a real-valued function, while $\mathcal{R}_2$ is a constant. Therefore, we reach the same conclusion: the winding number defined by Eq.3 of the main text for the third-order DP is 0.

Finally, we consider the 2D dissipative system, with the NH Hamiltonian

$$H = \begin{pmatrix} 0 & J_x - iJ_y \\ J_x + iJ_y & -i\gamma/2 \end{pmatrix}, \tag{S62}$$

where γ is the dissipation rate and $|J| = \sqrt{J_x^2 + J_y^2}$ is the coupling strength. This Hamiltonian has two EP2s at $J = \pm\gamma/4$. The characteristic polynomial is

$$P(E) = E^2 + i\gamma/2E - |J|^2, \tag{S63}$$

and its derivatives read

$$P'(E) = 2E + i\gamma/2, \tag{S64}$$

$$P''(E) = 2. \tag{S65}$$

From this, we can obtain the Sylvester matrices

$$S_{P,P'} = \begin{pmatrix} 1 & i\frac{\gamma}{2} & -|J|^2 \\ 2 & i\frac{\gamma}{2} & 0 \\ 0 & 2 & i\frac{\gamma}{2} \end{pmatrix} \text{ and } S_{P,P''} = \begin{pmatrix} 1 & i\frac{\gamma}{2} & -|J|^2 \\ 0 & 2 & 0 \\ 0 & 0 & 2 \end{pmatrix}. \tag{S66}$$

Subsequently, two components of the resultant vector $\mathcal{R}$ are given by

$$\mathcal{R}_1 = \gamma^2/4 - 4|J|^2, \tag{S67}$$

and

$$\mathcal{R}_2 = 4. \tag{S68}$$

Consistent with *Example 1* and *2*, $\mathcal{R}_1$ is a real-valued function, while $\mathcal{R}_2$ is a constant. As a result, along a closed loop around each EP2 in the $J_x - J_y$ parameter space, the corresponding winding number of $\mathcal{R}$ is 0.

These results confirm the claim of Ref. 12 of the main text that thus-defined winding number serves as a homotopy invariant, which uniquely characterizes the topology of EP3s.

---

[1] C. Song, S.-B. Zheng, P. Zhang, K. Xu, L. Zhang, Q. Guo, W. Liu, Da Xu, H. Deng, K. Huang, D. Zheng, X. Zhu, and H. Wang, Continuous-variable geometric phase and its manipulation for quantum computation in a superconducting circuit, Nat. Commun. 8, 1061 (2017).